13.11 VARIABILITY OF THE ARCTIC ATMOSPHERIC MOISTURE BUDGET DERIVED FROM TOVS SATELLITE DATA

[1]*David Groves and* [2]*Jennifer Francis**
[1]RAND Corporation, Santa Monica, California
[2]Rutgers University, New Brunswick, New Jersey

1. INTRODUCTION

The Arctic atmospheric moisture budget is an important component of the Arctic climate system, and hydrologic processes play a major role in governing interactions between the atmosphere and the Arctic Ocean. Miller and Russell [2000] also show that the Arctic hydrologic balance will be significantly affected by increasing greenhouse gas concentrations. Because long-term observations are sparse, however, and particularly measurements of moisture budget variables, it is difficult to confirm these model predictions.

Previous investigations have employed three distinct approaches: (1) climatologies based on measured precipitation and evaporation (e.g., Serreze and Hurst [2000] and Briazgin et al. [1996]), (2) moisture flux and flux convergence calculated from rawinsonde measurements (e.g., Nakamura and Oort [1988], Masuda [1990], Serreze et al. [1994], Walsh et al. [1994], Serreze et al. [1995b], and Serreze and Barry [2000]), and (3) moisture budget components derived from gridded reanalysis products and from forecast model output (e.g., Cullather et al. [2000], Bromwich et al, [2000], Serreze and Hurst [2000]) and Rogers et al. [2001]. The latter study used reanalyses from the National Centers for Environmental Prediction/National Center for Atmospheric Research (NCEP-NCAR) and from the European Centre for Medium-Range Weather Forecasts (ECMWF) to investigate patterns in moisture transport and net precipitation (P-E: precipitation minus evaporation/sublimation) corresponding with indices of several large-scale circulation patterns. They found significant regionally and seasonally varying correlations between P-E and the North Atlantic oscillation (NAO), Arctic oscillation (AO), and the North Pacific oscillation (NPO).

The AO is strongly related to the strength of the polar vortex and therefore is also related to the variability in lower-tropospheric winds. The AO index is positive (negative) when the SLP is anomalously low (high) over the poles and high (low) over the surrounding lower-latitude zonal ring. The AO accounts for 21% of the monthly SLP variance poleward of 20°N during November-April and 16% during May-October [Thompson and Wallace, 2000].

In this study we examine the temporal variability of the Arctic atmospheric moisture budget from a new 19-year (1980 to 1998), daily data set created by advecting daily satellite retrievals of precipitable water with upper-level wind fields from the NCEP-NCAR reanalysis data set. We examine the patterns of winter and summer moisture transport, decadal differences in the moisture budget, trends and interannual variability in moisture parameters, and relationships to variability in the AO. More detailed information about this work is presented in Groves and Francis [2002a,b].

* *Corresponding author address*: Jennifer Francis, Institute of Marine and Coastal Sciences, 71 Dudley Rd., Rutgers University, New Brunswick, NJ 08901-8521; e-mail: francis@imcs.rutgers.edu.

2. DATA AND METHODS

A daily, 19-year, gridded moisture budget data set for the Arctic atmosphere is created by combining TIROS Operational Vertical Sounder (TOVS) precipitable water (PW) retrievals [Francis and Schweiger, 2000; Schweiger et al, 2002] with NCEP-NCAR reanalysis gridded wind fields [Kalnay et al, 1996]. TOVS products have been extensively validated with measurements from the Russian "North Pole" data set and from the Surface Heat Balance of the Arctic (SHEBA) field experiment. Validation results are presented in Schweiger *et al.* [2002] and at http://psc.apl.washington.edu/pathp/pathp.html. We believe this approach is superior to one using PW fields from reanalyses for several reasons. First, the satellite moisture retrievals are relatively dense in space and time and are not subject to assimilation or interpolation schemes employed to create reanalysis and rawinsonde data sets. Second, rawinsondes over the central Arctic are few and far between, and are almost non-existent since the Russian program of North Pole drifting meteorological stations ended in 1991. Moreover, moisture retrievals from NOAA's operational TOVS processing system are *not* assimilated into the NCEP reanalysis over the Arctic, according to observation counts available on the NCEP-NCAR Reanalysis website. Confidence in the accuracy of reanalysis wind fields is higher, however, as more relevant data are assimilated, and there is no superior source of wind data for the Arctic region at this time. Surface pressure fields are well captured by autonomous buoys drifting on the sea ice as a part of the International Arctic Buoy Program [Rigor et al, 2000], and some satellite-derived temperature profiles aid in determining upper-level height fields. Consequently, we feel that the use of NCEP-NCAR wind fields is justified, while TOVS PW fields represent a substantial improvement over those from reanalyses.

All TOVS moisture variables are computed at $(100\ \text{km})^2$ horizontal resolution and at 16 vertical levels for each day from October 1979 to December 1998. Moisture products include precipitable water (PW), PW flux, PW flux convergence, and net precipitation, which is

calculated as the difference between PW flux convergence and PW tendency,

$$P - E = \frac{(-\nabla \bullet \vec{F})}{\rho_w} - \frac{\partial Q}{\partial t} \quad (1)$$

The P-E is precipitation minus evaporation/sublimation (net precipitation), $\vec{F}$ is the vertically integrated precipitable water mass flux, ρw is the density of liquid water, $(-\nabla \bullet \vec{F})/\rho_w$ is the vertically integrated precipitable water flux convergence, Q is the vertically integrated precipitable water (by volume), and Q/ tis its tendency. The dimension for each of the three terms in Eq. 1 is water volume per unit area per time, usually expressed as equivalent water depth per unit time.On annual time scales, precipitable water tendency is negligible and $(P - E) = (-\nabla \bullet \vec{F})/\rho_w$. For time periods shorter than a year, precipitable water tendency is not negligible [Groves and Francis, 2002a].

We separate total PW fluxes into components attributable to inter-monthly mean or large-scale circulation features (timescales > 30 days) and to high-frequency transient features (1 to 30 days). This is accomplished by calculating PW fluxes and flux convergences from monthly-mean wind and PW values, and subtracting these from the monthly means calculated from daily data. For further explanation, see Groves and Francis [2002].

We compute regional values of moisture budget parameters in the areas delineated in Fig. 1, which are consistent with those defined in previous studies of the Arctic Ocean freshwater budget [e.g., Steele et al, 1996].

Figure 1: Arctic Ocean regions used throughout the text. “Pacific sector” refers to regions 1-4, “Atlantic sector” to regions 8-9, and “Arctic basin” to regions 1-7.

To estimate relationships between seasonal moisture budget parameters and the AO index we use a least-squares linear regression following Thompson and Wallace [1998]. During the summer, when there is only a small trend in the AO index, we instead evaluate the extent to which variance in the AO explains the variance in a parameter by computing the squared correlation coefficient between the de-trended variable and the AO index. We construct composites of daily SLP, lower-troposphere winds, PW flux, and net precipitation for days with a positive (high), negative (low), and neutral AO index, classified according to whether it exceeds the long-term (1980-97) mean seasonal value by one standard deviation. In winter (summer), 35% (31%) of the days are classified as either high or low index days.

3. RESULTS

We find two major moisture/wind regimes over the Arctic: dry and anticyclonic during the cold months (November-March), and moist and cyclonic during the warm months (June-September). These well-defined differences in the PW and wind patterns between the two extreme seasons translate to differences in PW flux and PW flux convergence.

3.1 *Winter*

In winter (Nov-Mar), the mean geostrophic wind in the lower troposphere circulates clockwise around the Beaufort high, counter-clockwise around the Icelandic low, and across the Eurasian basin from the central Russian coast towards the Canadian Archipelago (islands in extreme northeast Canada), forming a distinctly zonally asymmetric pattern. The central Arctic is extremely dry during the winter with less than 2.5 mm of PW on average. Moisture amounts are slightly greater over the Chukchi Sea and Bering Strait owing to their proximity to open water in the Pacific Ocean, while PW is largest over the Barents Sea (~4 mm) and Norwegian Sea (~7 mm). The strongest gradients exist over the GIN and Barents Seas.

The PW flux (Fig. 2a) is strongly poleward over the western Pacific sector and equatorward over the eastern Pacific sector. Over the Atlantic sector PW flux is northeastward with meridional components ranging from 4 to 20 kg $m^{-1}s^{-1}$. Fig. 2b shows the flux of PW by transient circulation features. Over the GIN and Barents Seas, poleward transient fluxes range from 2 to10 kg $m^{-1}s^{-1}$, with the strongest fluxes between 70° and 80˚N. Nearly all of the poleward PW transport over the Pacific sector is caused by transient disturbances, which is consistent with winter storm tracks over the Arctic from 1979-85 [Serreze and Barry, 1988].

Total PW flux *convergence*, or equivalently (the calculated P-E from Eq. 1), is highest over the Atlantic sector, namely the GIN and Barents Seas, exceeding 3 cm mo^{-1} near Iceland and Norway (Fig. 2c). Net precipitation is smallest in the Beaufort Sea region and ranges between 0.5 and 1.0 cm mo-1 over most of the central Arctic. Over the Arctic basin as a whole (regions 1-7), transients provide 80% of the total, yet over the GIN Seas (region 9), they provide only 37% of the total (not shown). Transients dominate net precipitation over the central Arctic with very little structure in the corresponding PW flux field, suggesting that the moisture channeled into the Arctic via the North Atlantic storm track (affected by topography and ice/open water contrasts) is transferred to the surface throughout the entire eastern half of the Arctic basin rather than focussed into distinct areas. The result is a strong transient net precipitation signal

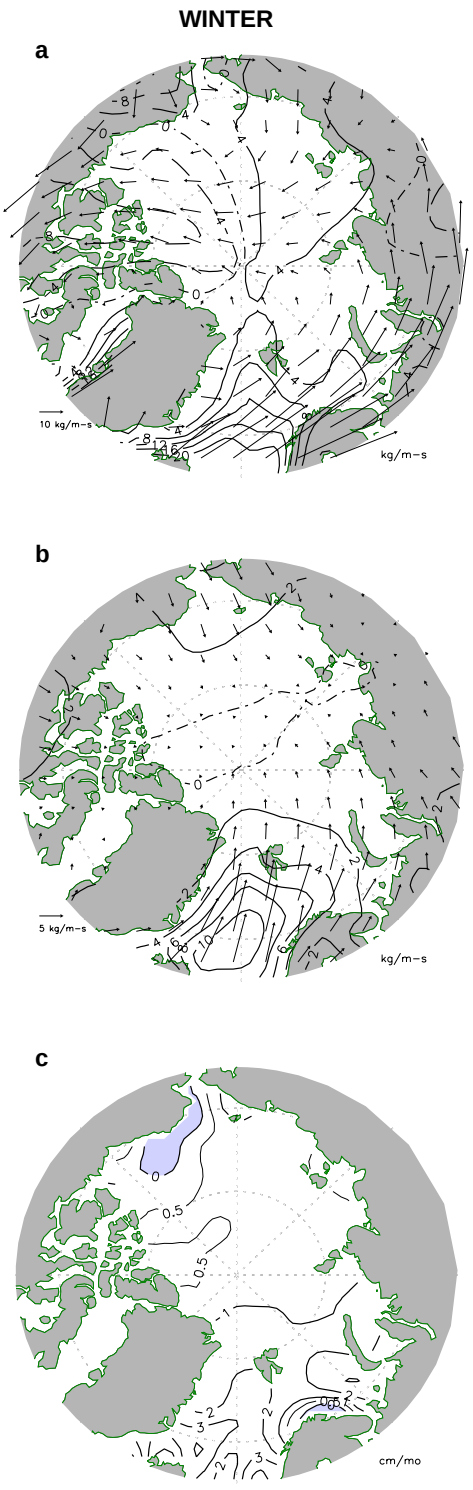

Figure 2: Winter (Nov-Mar, 1980-98) TOVS-derived moisture budget parameters: (a) total PW flux vectors and meridional fluxes (contour interval 4 kg m^{-1} s^{-1}), (b) PW flux vectors and meridional fluxes by transient features (contour interval 2 kg m-1s-1), and (c) P-E, where shaded regions are negative and contours are 0, 0.5, 1, 2, 3, and 4 cm mo^{-1}.

without a discernible corresponding PW flux pattern in winter over the central Arctic basin.

3.2 *Summer*

The mean SLP and circulation patterns during the warmest months (June-September) are dramatically different from those during the winter. A large, weak low-pressure system is centered almost directly over the North Pole, replacing the winter Beaufort high. The mean winds circulate counter-clockwise from the North Atlantic sector, where there are large amounts of atmospheric moisture, through the Russian, Chukchi, and Beaufort Seas and southward across the Canadian Archipelago.

During the summer, precipitable water exhibits a more axially symmetric pattern, with values less than 10 mm in the northern Canadian archipelago and from 12 to16 mm over the GIN Seas. Summer PW transport is also strongly zonal in much of the eastern Arctic (Fig. 3a), in the same direction as the mean lower-tropospheric winds. Strong meridional transport exists in the GIN and Chukchi Seas (northward) and over the Canadian archipelago (southward).

The summer high-frequency transient PW fluxes (Fig. 3b) are greater than those in winter (Fig. 2b) and are generally poleward throughout most of the Arctic, not only over the GIN and Chukchi Seas. As with the winter data, poleward flux is greatest near storm tracks, although summer tracks are less well delineated than in winter.

Summer PW flux convergence, or P-E, exceeds 2 cm mo^{-1} over most of the Arctic Basin (Fig. 3c), which is 3 times greater than during winter (Fig. 2c). Total summer P-E is more uniformly distributed than in winter, as is the contribution from transient features (not shown). The inter-monthly mean contributes the lion's share (42% of the total) in the GIN Seas.

The meridional PW transport across 70°N for the winter and summer seasons as well as the whole year is shown in Fig. 4. There are large seasonal differences in the amplitude of peaks over the GIN Seas (~20°E to 25°W), the dateline, and the Canadian archipelago (~60°W to 120°W). Despite the much stronger mean winds in winter, the poleward transport over the GIN Seas, for example, is substantially lower in winter (5.6 mm) than in summer (13.5 mm). While the strength and orientation of PW gradients do not differ markedly between the two seasons, the larger summer transport is primarily caused by the more poleward wind vectors and the increased depth of the moist layer.

3.3 *Arctic Oscillation and the Moisture Budget*

Relating the annual Arctic Oscillation Index to the annual moisture budget is problematic because the variance of the AO index is greatest during the winter and the variance of PW fluxes into the Arctic and net precipitation is greatest during the summer. Therefore, we investigate associations between the AO and the moisture budget only during the winter and summer seasons. Winter is defined as January-March, summer as July-September, and we analyze the 18-year period from

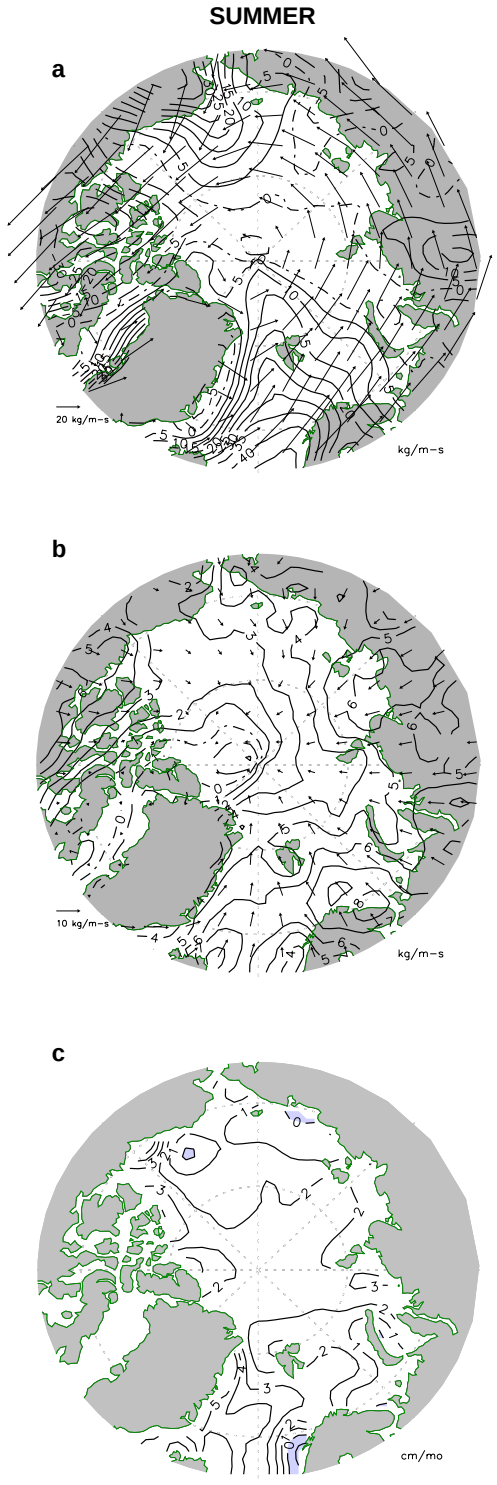

Figure 3: Summer (Jun-Sept, 1980-98) TOVS-derived moisture budget parameters: (a) total PW flux vectors and meridional fluxes (contour interval 4 kg m^{-1} s^{-1}), (b) PW flux vectors and meridional fluxes by transient features (contour interval 2 kg $m^{-1}s^{-1}$), and (c) P-E, where shaded regions are negative and contours are 1 cm mo^{-1}.

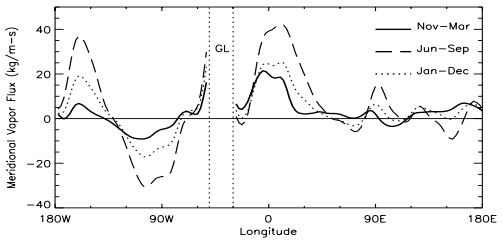

Figure 4: Mean meridional precipitable water flux across 70° N during the winter (Nov.-Mar.), summer (Jun.-Sept.), and all months from TOVS (1980-98). "GL" indicates the longitudes bounding the Greenland continent

1980 to 1997. High (positive) and low (negative) index days are composited. Positive AO days are characterized by strong cross-basin flow from Eurasia to the Canadian Archipelago. On low-index days the low-tropospheric winds are cyclonic in the Atlantic sector, and the flow regime is primarily equatorward over the GIN and Chukchi Seas and anticyclonic over the Arctic basin as a whole.

On high index days (Fig. 5a), the PW flux is similar in structure to, but stronger than, the mean winter PW flux. On low index days (Fig. 5b), the average PW flux pattern is considerably weaker, and more westerly fluxes exist over the GIN and Barents Seas. The similarity in winter PW fields on high and low index days suggests that the often shallow layer of moisture near the surface is controlled primarily by surface processes, rather than large-scale circulation effects. It also suggests that variations in the PW flux on high and low index days are governed by differences in the wind field.

The meridional profile of PW flux across 70˚N (Fig. 6) quantifies the larger poleward PW fluxes over the Atlantic sector and enhanced equatorward fluxes over the Canadian Archipelago on high index days. Integrating over longitude reveals that during winter, the net PW flux across 70˚N is six times greater on high AO-index days than on low AO-index days and 63% greater than the mean over all days. The strongly contrasting PW flux regimes on high and low AO-index days result in large differences in net precipitation (Fig. 7). Over the Arctic basin as a whole P-E exceeds the mean on high AO-index days by 29% and falls below the mean on low AO-index days by 20%. The Beaufort Sea experiences much higher net precipitation on high-index days.

Trends in TOVS-derived winter P-E are largest over the GIN and Barents Seas with a maximum of 1.5 mm mo^{-1} yr^{-1}. This represents 38% of the seasonal mean, and 66% is linearly congruent with the AO. In the Pacific sector, trends are largest over the Beaufort Sea (exceeding 0.5 mm mo^{-1} yr^{-1}). This 18-year change is 103% of the mean winter value, and 40% of it is linearly congruent with the AO. Slightly negative trends are present over the Barents Sea and near the pole, extending over the Canadian Archipelago. Over the Arctic basin as a whole, the 18-year trend is 27% of the seasonal mean and 55% is linearly congruent with the AO.

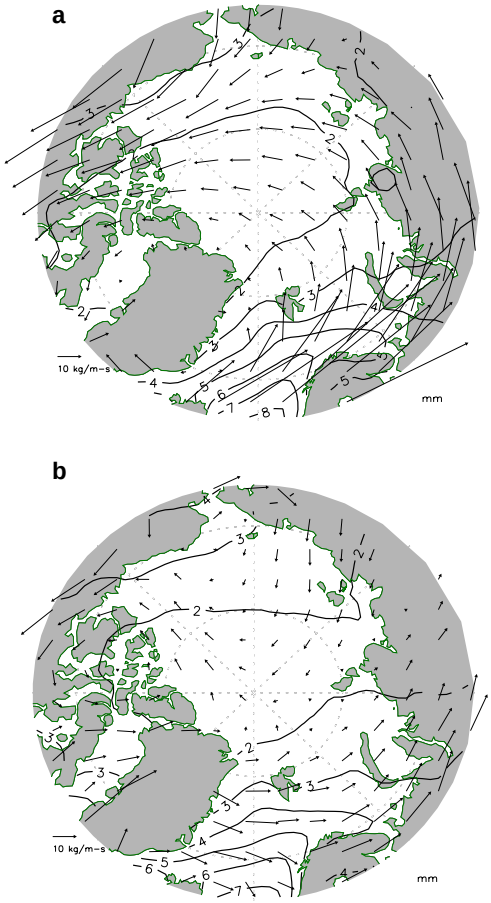

Figure 5: (a) High and (b) low AO composite map of PW (contours) and PW flux (vectors) during winter.

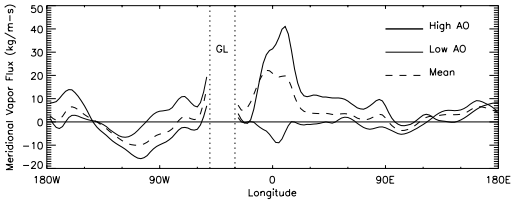

Figure 6: Meridional winter PW flux across 70° N on high (thick, solid) and low (thin, solid) AO-index days, and for the seasonal mean (dashed) for 1980-97. "GL" indicates the longitudes bounding Greenland

In summer the difference in PW on high versus low AO-index days is striking, with larger values almost everywhere and particularly over marginal seas in the eastern Arctic. On high-index days, cyclonic flow centered over the pole drives strong poleward PW fluxes over the GIN, Barents, and Beaufort Seas (Fig. 8a). PW flux on low AO-index days is considerably weaker (Fig. 8b), with coherent poleward fluxes only over the Nansen Basin, North Pole, and Canada Basin. The resulting P-E is predominantly larger on high-index days

Figure 7: Difference in winter P-E between composited high and low AO index days (high-low).

(Fig. 9) particularly in the Atlantic and eastern Pacific sectors.

Figure 10 shows the summer poleward PW flux across 70˚N for high and low AO-index days and the seasonal mean. On high AO-index days, poleward fluxes are larger over the Atlantic sector (30˚E-40˚W) and central Russia (~90˚E), and equatorward fluxes are stronger west of Greenland and over the Canadian Archipelago (70˚W-55˚W). Integrating around 70˚N reveals that the total poleward flux in summer on high AO-index days is about double that of low AO-index days. The summer pattern of P-E for the high minus low AO-index composite (not shown) is less coherent than the wintertime pattern. Net precipitation is 12% greater than the seasonal mean on high AO-index days and 15% lower on low AO-index days.

Trends in the AO pattern as well as net precipitation over the Arctic basin are insignificant during summer. Regions with the greatest summer interannual variation in P-E from 1980 to 1997 are the GIN and Barents Seas, and the coastal regions of the Beaufort, Chukchi, and Laptev Seas, which are also the areas of large summer P-E. The central Canada basin has the least amount of variability. The AO's contribution to variability in P-E is largest over the Pacific and Atlantic sectors, where 62% and 47% of the variability is linearly congruent with the AO, which translates to 38% and 22% of the variance being explained by the AO.

4. CONCLUSIONS

Sea level pressure and upper-level winds obtained from the NCEP-NCAR Reanalysis have been combined with fields of precipitable water retrieved from the TOVS Path-P data set to produce new estimates of moisture transport and net precipitation over the Arctic Ocean. We have analyzed and compared values for winter and summer seasons and determined that the calculated PW flux and net precipitation fields are strongly influenced by both the mean circulation regime and by transient features. The importance of each of these components var-

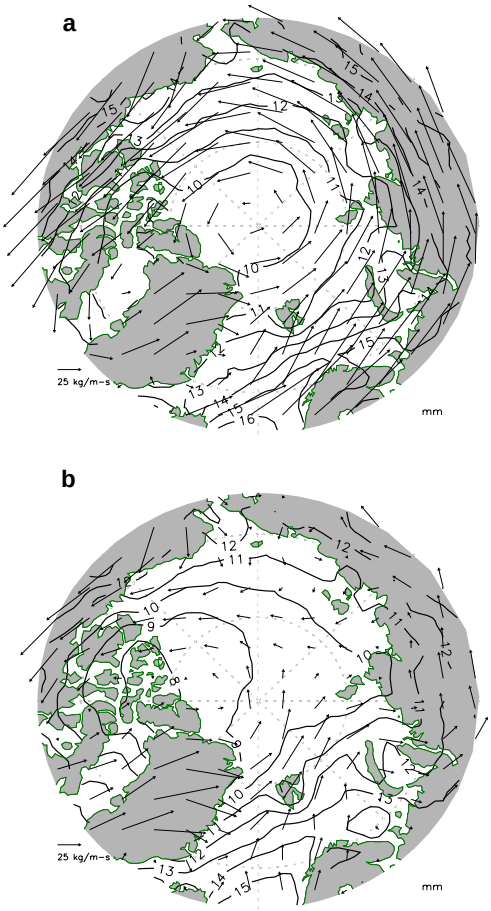

Figure 8: (a) High and (b) low AO composite map of PW (contours) and PW flux (vectors) during summer.

ies seasonally and regionally. Seasonal differences in the moisture budget result from the interaction of seasonally distinct circulation regimes and PW patterns. In winter, the atmosphere is extremely dry, with ~2.5 mm of PW over sea ice-covered areas. Meridional moisture gradients, however, are strong and confined primarily to the GIN/Barents Seas and Bering Strait area. In contrast, the summer low-level wind flow is weaker and much less coherent, with a generally cyclonic circulation around the Arctic basin. The PW amounts are approximately 5 times higher in summer than in winter on average. Summer meridional PW gradients are just as strong as in winter but are more zonally symmetric.

The spatial patterns of PW flux and net precipitation are also very different in winter and summer. During winter moisture follows the mean low-level flow pattern and enters the Arctic along two primary pathways: from the GIN seas into the Barents and Kara seas, and also from Russia across the Laptev and Chukchi seas towards the Canadian Archipelago. Both PW flux pathways are due primarily to transient circulation features. Transient features are also responsible for most of the PW flux convergence over all areas (~80%), except in the GIN Sea

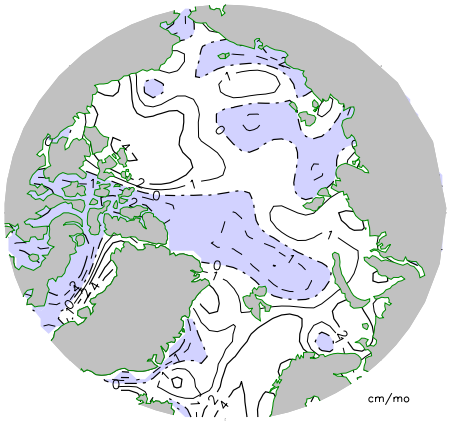

Figure 9: Difference in summer P-E between composited high and low AO index days (high-low).

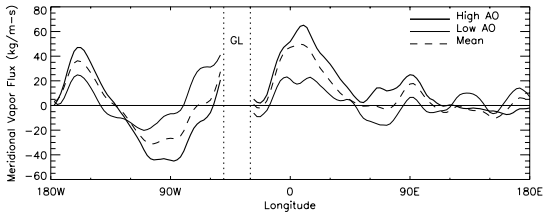

Figure 10: Meridional summer PW flux across 70° Non high (thick, solid) and low (thin, solid) AO-index days, and for the seasonal mean (dashed) for 1980-97. “GL” indicates the longitudes bounding Greenland

(~37%) where the mean flow is dominated by the semi-permanent Icelandic low pressure center.

Winter P-E is generally light, ranging from 3 cm mo^{-1} near the Atlantic marginal ice zone to less than 1 cm mo^{-1} over the central Arctic. During summer, in contrast, transient systems enter the polar cap from all surrounding regions except the Canadian Archipelago and Greenland. Summer PW flux convergence is accomplished mostly by transient features (~68%), and net precipitation is almost double that of winter and more uniformly distributed, ranging from 2 to 4 cm mo^{-1}. The annual moisture budget is dominated by summer transport.

The AO index explains a significant amount of variability in both PW fluxes and net precipitation ($r = 0.31$; correlated with > 99% confidence), especially during winter. The strongest effects are evident over the Atlantic sector, where increased westerlies, which characterize the positive-phase AO, advect greater amounts of moisture into the Arctic. We find significant trends in winter net precipitation, particularly in the GIN/Barents Seas and Pacific sector. In the GIN/Barents Seas the 18-year trend represents 38% of the seasonal mean, of which 66% is linearly congruent with the AO index. In the Pacific sector, the 18-year change is 103% of the mean winter value. Over the entire Arctic basin the trend is 27% of the winter mean, and 55% is linearly congruent

with the AO. This suggests that observed trends in the winter AO index toward the positive phase contribute toward increased net precipitation in winter.

Winter PW fluxes vary with AO phase while PW amounts do not, confirming the circulation's important role in transporting moisture. Over the Arctic basin as a whole in winter, P-E is 29% greater than the climatological average on high AO-index days and 20% lower than climatology on low index days. On positive AO-index days, the net PW flux across 70°N is 6 times larger than on low-index days, and it is 63% larger than the mean for all days.

During summer, the cyclonic circulation present in the seasonal and monthly means is strengthened on high AO-index days. The PW transport into the Arctic, consequently, is twice as large during periods with a positive AO index. Net precipitation also increases throughout the Arctic (12% greater than the 18-year mean), while on low-index days it is 15% lower than the seasonal mean. These results suggest that AO variability is a dominant mechanism driving interannual variability in the moisture budget during summer as well as in winter.

Finally, our analysis suggests that if the AO continues to reside in a primarily positive phase, we should expect to find increased precipitation in the Arctic basin as a whole, and particularly in areas adjacent to marginal ice zones. This increased flux of freshwater into the Arctic may eventually affect sea ice thickness, although the overall result is uncertain owing to the counteracting effects of snow cover on sea ice. Increased net precipitation may also affect the freshwater outflow by increasing the amount of snow on top of the sea ice.

5. REFERENCES

Briazgin, N. N., L. P. Burova, V.P. Khrol, *Atlas of the water balance of the northern polar area* (in Russian). Arctic and Antarctic Research Institute. St. Petersburg, *Progress-Pogoda, Gidrometeoizdat*, 82 pp., 1996.

Bromwich, D.H., R.I. Cullather, and M.C. Serreze, Reanalysis depictions of the Arctic atmospheric moisture budget. *The Freshwater Budget of the Arctic Ocean*, E.L. Lewis, ed., Kluwer Academic Publishers, Kluwer, The Netherlands, 163-196, 2000.

Cullather, R. I., D.H. Bromwich, and M.C. Serreze, The atmospheric hydrologic cycle over the Arctic Basin from reanalysis. Part I: Comparison with observations and previous studies. *Journal of Climate*, 13, 923–37, 2000.

Francis, J. A. and A.J. Schweiger, A new window opens on the Arctic. *EOS Transactions*, 81(8), 77-83, 2000.

Groves, D.G. and J.A. Francis, The moisture budget of the Arctic atmosphere from TOVS satellite data, *J. Geophys. Res., D19*, 4391, doi:10.1029/2001JD001191, 2002a.

Groves, D.G. and J.A. Francis, Variability of the Arctic Atmospheric Moisture Budget from TOVS Satellite Data, *J. Geophys. Res., D24,* 4785, doi:10.1029/2002JD002285, 2002b.

Kalnay, E., M. Kanamitsu, R. Kistler, W. Collins, D. Deaven, L. Gandin, M. Iredell, S. Saha, C. White, J. Woollen, and Zhu, The NCEP/NCAR 40-year reanalysis project. *Bull. Am. Meteorol. Soc.*, 77(3), 437–71, 1996.

Masuda, K., Atmospheric heat and water budgets of the polar regions: analysis of FGGE data. *Proceedings of the NIPR Symposium on Polar Meteorology and Glaciology, 3,* 79-88, 1990.

Miller, J.R. and G.L. Russell, Projected impact of climatic change on the freshwater and salt budgets of the Arctic Ocean by a GCM, *Geophys. Res. Lett, 27*, 1183-86, 2000.

Nakamura, N. and A. H. Oort, Atmospheric heat budgets of the polar regions. *J. Geophys. Res., 93,* 9510-9524, 1988.

Rigor, I. G., R.L. Colony, and S. Martin, Variations in surface air temperature observations in the Arctic, 1979–97. *J. Climate*, 13, 896–914, 2000.

Rogers, A. N., D. H. Bromwich, E. N. Sinclair, and R. I. Cullather, The atmospheric hydrologic cycle over the Arctic basin from reanalyses. Part II: Interannual variability. *J. Climate, 14,* 2414-2429, 2001.

Schweiger, A.J., R.W. Lindsay, J.A. Francis, J. Key, J. Intrieri, and M. Shupe, Validation of TOVS Path-P data during SHEBA. *J. Geophys. Res., 107(C10),* 8041, 10.1029/2000JC000453, 2002.

Serreze, M. C., and C.M. Hurst, Representation of mean Arctic precipitation from NCEP-NCAR and ERA Reanalyses. *Journal of Climate, 13,* 182–201, 2000.

Serreze, M. C., and R.G. Barry, Atmospheric components of the Arctic Ocean hydrologic budget assessed from rawinsonde data. *The Freshwater Budget of the Arctic Ocean,* E. L. Lewis, ed., Kluwer Academic Publishers, Kluwer, The Netherlands, 141-161, 2000.

Serreze, M. C., M.C. Rehder, R.G. Barry, and J.D. Kahl, A climatological data base of Arctic water vapor characteristics. *Polar Geography and Geology*, 18(1), 63–75, 1994.

Serreze, M. C., M.C. Rehder, R.G. Barry, J.D. Kahl, and N.A. Zaitseva, The distribution and transport of atmospheric water vapor over the Arctic basin. *International Journal of Climatology*, 15(7), 709–27, 1995b.

Serreze, M. C., and R.G. Barry, Synoptic activity in the Arctic Basin, 1979–85. *J. Climate*, 1(12), 1276–95, 1988.

Steele, M., D. Thomas, D. Rothrock, and S. Martin, A simple model study of the Arctic Ocean freshwater balance, 1979–1985. *J. Geophys. Res.*, 101(C9), 20,833–48, 1996.

Thompson, D. W. J., and J. M. Wallace, Annular Modes in the Extratropical Circulation. Part I: Month-to-Month Variability. *J. Climate*, 13, 1000–16, 2000.

Thompson, D. W. J., and J. M. Wallace, The Arctic Oscillation signature in the wintertime geopotential height and temperature fields. *Geophys. Res. Lett.*, 25(9), 1297–300, 1998.

Walsh, J. E., X. Zhou, D. Portis, and M. C. Serreze, Atmospheric Contribution to Hydrologic Variations in the Arctic. *Atmosphere-Ocean*, 32(4), 733–55, 1994.

Acknowledgements. This work was supported by an NSF Graduate Research Fellowship, NASA Grants NAGW-2407 (POLES) and NAG5-11720, and NSF Grant SGER: 0105461. The authors would like to thank Drs. Drew Rothrock, Mike Wallace, David Battisti, and Axel Schwieger for their extensive suggestions and guidance, and Mr. Mark Ortmeyer for computing support.